JOURNAL OF GEOPHYSICAL RESEARCH, VOL. 114, B06210, doi:10.1029/2008JB006185, 2009

Melt channelization in ascending mantle

I. J. Hewitt[1] and A. C. Fowler[1,2]

Received 30 October 2008; revised 14 March 2009; accepted 28 April 2009; published 27 June 2009.

[1] We study a model for channels of magma flow within mantle undergoing decompression melting. Cylindrical conduits in a viscous, porous, compacting matrix are considered, and it is found that the dynamics of the conduit walls are governed by the competition between melting (caused by decompression) and viscous closure (caused by the reduced pressure in the conduit). There are many similarities with the Röthlisberger channels which transport melt water beneath glaciers. Pressure in these mantle conduits is very nearly magmastatic, and ascent velocities on the order of 100 m a^{-1} are predicted. Flow from the surrounding porous partially molten matrix into the low-pressure channel is considered and can supply a continual source of melt. The accumulation region is on the order of the compaction length, and the residual matrix is reduced to very low melt fractions, typically <0.5%. Channels form naturally from porous flow in the matrix because of the enhanced melting rate in regions of higher porosity, which have a larger heat flux from below. The vast majority of melt could be expected to flow eventually into one of these channels, which therefore offer a physical grounding for the conceptual near-fractional melting models used to explain field observations.

Citation: Hewitt, I. J., and A. C. Fowler (2009), Melt channelization in ascending mantle, *J. Geophys. Res.*, *114*, B06210, doi:10.1029/2008JB006185.

1. Introduction

[2] Magma production beneath mid-ocean ridges and in mantle hotspots occurs because of the decompression melting of the upwelling mantle rock. The rock is believed to melt along grain boundaries which results in a partially molten solid matrix with melt-filled pores. The positively buoyant melt can then rise slowly through the matrix while the matrix deforms, or compacts, to accommodate this. There are, however, several geochemical and geophysical reasons to suggest that this type of porous flow is not the main extraction mechanism for melt from these melting regions, and that instead the melt can segregate from the matrix and rise in localized high-porosity channels [*Kelemen et al.*, 1997]. This paper aims to study the dynamics of open-melt conduits in a viscous compacting porous matrix undergoing decompression melting.

[3] Whether such open melt channels exist in the mantle is not known, and one of the purposes of this study is to examine, at least from a fluid mechanical point of view, whether they are viable. Mechanisms which could produce open conduits include ''fracturing'' of the partially molten matrix [*Nicolas*, 1986], and mechanical or reactive instabilities to the flow [*Stevenson*, 1989; *Aharonov et al.*, 1995; *Spiegelman et al.*, 2001].

[4] The evidence for focussed, chemically isolated flow of magma from within the mantle is well documented [*Kelemen et al.*, 1997; *Iwamori*, 1993; *Asimow and Stolper*, 1999]; erupted MORB (the solidified melt) is not in chemical equilibrium with the residual mantle peridotite, and is inferred to have been transported from deep within the partially molten region in various degrees of chemical isolation from the residual matrix. This is inconsistent with porous flow and has led to many conceptual ''two porosity'' models of melt extraction termed ''fractional'' or ''near-fractional'' melting, the idea being that melt is produced in the pores in equilibrium with the surrounding matrix, but is then instantaneously or nearly instantaneously extracted to higher levels so that its chemical signature is preserved [*Asimow and Stolper*, 1999; *McKenzie*, 1985; *Iwamori*, 1993]. High-porosity or open melt channels potentially provide a mechanism for doing this.

[5] The emphasis in this paper is on the underlying driving mechanism for melting and how this plays a role in determining the type of melt flow. We are considering areas of upwelling mantle where the temperature of the ascending rock intersects the pressure-dependent solidus; it is then constrained to the solidus and the excess heat contained in the ascending rock is what drives melting. From this standpoint, it is really the rate of upwelling of *heat* from the hotter mantle below which determines how much melting occurs, and the crucial point we want to emphasize is that this heat is carried by both the ascending matrix and the ascending melt. In an open channel, or even in high-porosity regions in the partial melt, the *melt* provides the main heat transport and this has a significant impact on the governing dynamics. Indeed it can lead to a ''runaway'' effect which essentially erodes an open channel in a previously low porosity matrix. The governing equations are very similar to those for the well-known reaction-infiltration

[1]Mathematical Institute, University of Oxford, Oxford, UK.
[2]Department of Mathematics and Statistics, University of Limerick, Limerick, Ireland.

0148-0227/09/2008JB006185$09.00

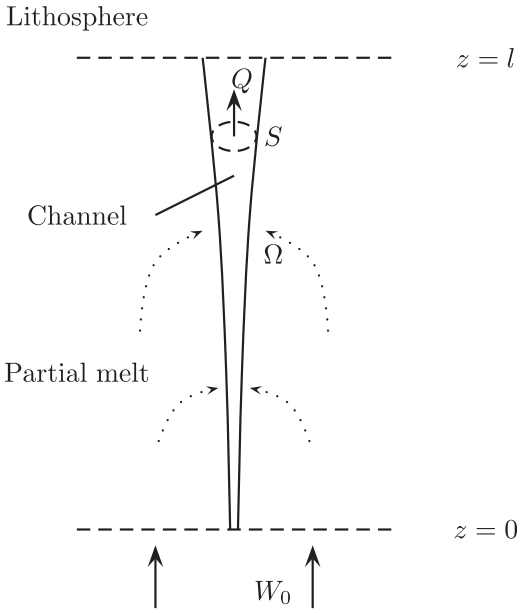

Figure 1. Geometry considered in sections 2 and 3. Mantle rock is ascending with velocity W_0 and begins to partially melt at $z = 0$. The top of the partially molten region (the base of the lithosphere) is at $z = l$; the effective pressure is prescribed to be zero there. The melt rising up the channel may either pond and subsequently freeze on to the base of the lithosphere, or continue to ascend through dykes. The channel shown extends the full depth of the partial melt, as is assumed in section 2; its width is greatly exaggerated. Melt is drawn from the surrounding porous partial melt as shown by the dotted arrows and results in a source Ω to the channel.

instability, but involve only a single component rock whose melting rate is determined by a consistent conservation of energy.

[6] For the sake of simplicity, and in an attempt to keep these ideas clear, we will ignore all compositional effects and treat the mantle as a single component rock. The solidus in this case will be a function of pressure only; later we consider the concentration of incompatible trace elements, but we do not take account of compositional effects on the solidus. Whilst a vast simplification of the real mantle, we believe that the insights that can be gained from this approach are helpful.

[7] Studies of magma conduits in the mantle have been made in the past; experiments have been conducted by injecting light viscous fluids into more viscous ones and comparing the laboratory observations with theory [*Helfrich and Whitehead*, 1990; *Olson and Christensen*, 1986]. Much of the interest has been with solitary waves that travel up such conduits and for which the experiments and theory are in good agreement. *Richardson et al.* [1996] considered conduit flow within a viscous porous medium, and studied the flow into and out of a conduit during the passage of a solitary wave.

[8] Little attention has been paid to how melt gets into a putative conduit from the surrounding region of partial melt. It is evidently crucial that this type of inflow is possible, since supplying a lumped flux at the conduit base seems unrealistic. *Sleep* [1988] considered how melt flow in a compacting partially molten matrix might be sucked into small low-pressure veins and dikes and found that this could be done over distances comparable to the *compaction* length, which is the length scale over which pressure variations are felt in the surrounding partial melt. In section 3 we similarly consider the flow into a channel, but we first examine how the channels themselves might operate once formed.

[9] Section 2 studies the dynamics of a conduit of magma surrounded by a more viscous matrix. The important addition to previous models is to take account of the additional melting which occurs as the melt ascends within the conduit. We find that this added melting has a controlling effect on how a channel ultimately evolves, and the situation is very similar to that which is well known for channels of melt water in the basal regions of glaciers [*Röthlisberger*, 1972; *Nye*, 1976]: the size of the channel is governed by a balance between the walls melting and deforming by viscous closure. In the glacier case the melting is driven by viscous dissipation of the turbulent water flow, whereas here it is driven by laminar advection down the solidus gradient. Both these scenarios have the effect of providing a melting rate proportional to the flow rate.

[10] After considering the feeding supply of melt from the partially molten matrix in section 3, section 4 looks at how a channel might naturally evolve out of an instability to the porous flow, while in section 5 we discuss some implications of these results.

2. Channel Dynamics

[11] We consider a vertical conduit filled with viscous fluid (that is, melt) of density ρ_l and pressure p_c contained in a more viscous fluid (the "solid" matrix) of density ρ_s and pressure p_s. The conduit is assumed to be cylindrical, with cross-sectional area $S(z, t)$, and vertical volume flux $Q(z, t)$. Geophysically, we envisage the channel embedded within a partially molten region of the decompressing mantle, as shown in Figure 1. The cylindrical shape is chosen since a channel forming through dissolution or melting instabilities might be expected to be symmetric, or if it forms through fracturing of the matrix, the initially planar shape can be expected to localize into a series of cylinders as a result of nonuniform melting of the walls [cf. *Bruce and Huppert*, 1990]. The pressure in the matrix is lithostatic $p_s = p_0 - \rho_s g z$, and we write the pressure reduction in the melt as the *effective* pressure $N_c \equiv p_s - p_c$. The Reynolds number is small, so the flow is laminar, governed by the Poiseuille law

$$Q = \frac{S^2}{8\pi\eta_l}\left(\Delta\rho g + \frac{\partial N_c}{\partial z}\right), \tag{1}$$

where η_l is the melt viscosity, $\Delta\rho = \rho_s - \rho_l$ is the density difference and g is the gravitational acceleration. The continuity equation for the melt is

$$\frac{\partial S}{\partial t} + \frac{\partial Q}{\partial z} = \frac{M}{\rho_l} + \Omega, \tag{2}$$

in which M (kg m^{-1} s^{-1}) is the rate of melting of the channel walls, and the source term Ω is included to account for the

Table 1. Values of Model Constants

Parameter	Value
g	10 m s^{-2}
ρ_s	3×10^3 kg m^{-3}
ρ_l	2.5×10^3 kg m^{-3}
c	10^3 J kg^{-1} K^{-1}
k	2.5 J m^{-1} s^{-1} K^{-1}
L	3×10^5 J kg^{-1}
Γ	10^{-7} K Pa^{-1}
α	20
k_0	4×10^{-9} m^2
η_l	1 Pa s
η_s	3×10^{18} Pa s
l	50 km
W_0	10^{-9} m s^{-1}

inflow of melt through the (small) pores in the walls; this is taken as arbitrary in this section, but will be calculated from the surrounding porous flow in section 3.

[12] The melt pressure is related to the movement of the channel walls, since an inclusion at reduced pressure N_c in a fluid of viscosity η_s will close down at a rate [*Nye*, 1953; *Sleep*, 1988]

$$\frac{\partial S}{\partial t} = -\frac{SN_c}{\eta_s} \equiv -\frac{S(p_s - p_c)}{\eta_s}. \tag{3}$$

However, the melting of the walls causes S to grow, so the kinematic condition for the conduit walls is really

$$\frac{\partial S}{\partial t} = \frac{M}{\rho_s} - \frac{SN_c}{\eta_s}. \tag{4}$$

This evolution equation allows for a steady state in which the rate of viscous closure caused by the pressure difference matches the melting rate. It is left to determine this melting rate, and it must come from energy considerations.

[13] The conduit walls are assumed to be at the melting temperature (solidus) T_s, which is pressure, and therefore depth, dependent. This is because heat conduction on the scale of the pores is fast enough to constrain the matrix to thermodynamic equilibrium. If we assume a linear Clapeyron slope Γ, we have

$$T_s = T_0 - \Gamma(\rho_s g z + N_c), \tag{5}$$

where the term in brackets is $p_0 - p_c$; p_c being the interfacial pressure, and T_0 and p_0 being a reference temperature and pressure. We allow for the fact that the temperature in the conduit may be different from the wall temperature by writing the average temperature there as $T = T_s + \theta$. θ is thus the average temperature *excess* in the ascending melt (the actual temperature will be hotter in the center and equal to the wall temperature at the edges). Energy conservation is expressed as

$$ML + \rho_l c S \frac{\partial}{\partial t}(T_s + \theta) + \rho_l c Q \frac{\partial}{\partial z}(T_s + \theta) = Q\left(\Delta\rho g + \frac{\partial N}{\partial z}\right), \tag{6}$$

in which the first term is the energy lost to melting the walls, the rest of the left hand side is heat advection, and the term on the right hand side is heating by viscous dissipation. L is the latent heat of melting and c is the specific heat capacity. The melting rate is related to the temperature excess by an energy transfer equation

$$ML = \alpha k \theta, \tag{7}$$

for conductive heat transfer enhanced by advection in a cylindrical pipe. α is a constant and k is the thermal conductivity of the melt. Note that heat conduction is important for the energy transfer into the walls, but does not appear (except implicitly through M) in equation (6) which has been averaged over the channel cross section. Vertical heat conduction is negligible.

[14] Equations (1), (2), (4), (5), (6) and (7) provide a closed system for the flux, cross section, effective pressure, temperature and melting rate. If melting is ignored (so temperature must also be ignored) and $\Omega = 0$, equation (3) gives the effective pressure, which can be substituted into equations (1) and (2) to give

$$Q = \frac{S^2}{8\pi\eta_l}\left(\Delta\rho g + \eta_s \frac{\partial}{\partial z}\left(\frac{1}{S}\frac{\partial Q}{\partial z}\right)\right). \tag{8}$$

This, in combination with the continuity equation (2), gives equations which have often been used to describe solitary waves on fluid conduits [*Olson and Christensen*, 1986; *Helfrich and Whitehead*, 1990]. In the small perturbation limit it reduces to the Korteweg de-Vries equation with soliton solutions [*Whitehead and Helfrich*, 1986].

[15] On the face of it, one might think that the melt rises buoyantly and that for a typical area S_0 the flux is therefore of magnitude, from equation (1),

$$\frac{S_0^2 \Delta\rho g}{8\pi\eta_l}. \tag{9}$$

For a cross-sectional area 1 m^2, and using the typical values in Table 1, this gives melt velocities of around 200 m s^{-1}. This is much too large to account for the rate of crustal accretion at mid ocean ridges and led *Kelemen et al.* [1997], for instance, to conclude that open channels of this sort must be transient, if they exist at all. However, the dynamics of these channels can be quite different if the pressure in them is closer to equilibrium; *magmastatic* equilibrium occurs if the pressure increases with depth because of the weight of the overlying magma or, in terms of the effective pressure,

$$\frac{\partial N_c}{\partial z} = -\Delta\rho g. \tag{10}$$

For the steady state considered here, the dominant balance in equation (1) turns out to be between these terms on the right hand side, so that the flow is driven not by the full buoyancy force $\Delta\rho g$ but only a small fraction of it. The size of the channel is determined by the balance between melting and viscous closure in equation (4). The melting rate is determined from the energy equation (6) and is essentially given by the rate at which melt is advected down the solidus gradient, the heat transfer to the walls being so efficient as

to prevent the melt in the conduit from rising significantly above the wall temperature.

[16] These important balances motivate scaling the variables according to

$$T_s - T_0 \sim \Gamma \rho_s g z, \quad N_c \sim \Delta \rho g z, \quad ML \sim \rho_l c \Gamma \rho_s g Q, \quad \frac{M}{\rho_s} \sim \frac{SN_c}{\eta_s}, \quad ML \sim \alpha k \theta. \tag{11}$$

This gives rise to scales, denoted by a subscript 0,

$$T_{s0} = \Gamma \rho_s g l, \quad N_{c0} = \Delta \rho g l, \quad M_0 = \rho_l \frac{c \Gamma \rho_s g}{L} Q_0, \quad S_0 = \frac{\rho_l}{\rho_s} \frac{\eta_s}{\Delta \rho g l} \frac{c \Gamma \rho_s g}{L} Q_0, \quad \theta_0 = \frac{\rho_l}{\alpha k} c \Gamma \rho_s g Q_0, \tag{12}$$

in terms of a typical length scale l and melt flux Q_0, which can either be prescribed at the lower end of the conduit, or determined from the rate of inflow Ω_0 by $Q_0 = \Omega_0 l$.

[17] Scaling all the variables as in equation (12), and the time according to $t_{c0} = \eta_s / N_{c0}$, results in the nondimensional equations

$$\frac{\partial S}{\partial t} = M - S N_c, \tag{13}$$

$$\frac{1}{rSt} \frac{\partial S}{\partial t} + \frac{\partial Q}{\partial z} = \frac{1}{St} M + \Omega, \tag{14}$$

$$\Lambda Q = S^2 \left(1 + \frac{\partial N_c}{\partial z} \right), \tag{15}$$

$$M + \frac{1}{rSt} S \frac{\partial}{\partial t} (T_s + \mu \theta) + Q \frac{\partial}{\partial z} (T_s + \mu \theta) = \nu Q \left(1 + \frac{\partial N_c}{\partial z} \right), \tag{16}$$

$$T_s = -z - \frac{r-1}{r} N_c, \tag{17}$$

$$\theta = M, \tag{18}$$

in which the dimensionless parameters are

$$r = \frac{\rho_s}{\rho_l}, \quad St = \frac{L}{c \Gamma \rho_s g l}, \quad \mu = \frac{\theta_0}{\Gamma \rho_s g l}, \quad \nu = \frac{\Delta \rho}{\rho_s \rho_l c \Gamma}, \quad \Lambda = \frac{8 \pi \eta_l}{\Delta \rho g} \frac{Q_0}{S_0^2}. \tag{19}$$

r is the density ratio, St is a Stefan number, which is the ratio of latent heat to sensible heat (in this case given by the change in the solidus temperature up the conduit $\Gamma \rho_s g l$), and μ is the ratio of excess channel temperature to this range of the solidus. ν measures the importance of viscous dissipation and Λ measures the deviation of the melt pressure from magmastatic caused by the fluid flow.

[18] We suppose for the moment that the channel flux is of order $Q_0 = 0.01$ m^3 s^{-1}, and that the conduit occupies the full depth of the partial melt with length $l = 50$ km. With the other parameters as in Table 1, this gives

$$N_{c0} \approx 2.5 \times 10^8 \text{ Pa} \quad M_0 \approx 2.5 \times 10^{-4} \text{ kg m}^{-1} \text{ s}^{-1} \quad S_0 \approx 1000 \text{ m}^2, \quad T_{s0} \approx 150 \text{ K}, \quad \theta_0 \approx 1.5 \text{ K}, \quad t_{c0} \approx 1.2 \times 10^{10} \text{ s} \approx 400 \text{ a}. \tag{20}$$

The dimensionless parameters are then

$$r \approx 1.2, \quad St \approx 2, \quad \mu \approx 0.01, \nu \approx 0.7, \quad \Lambda \approx 5 \times 10^{-11}. \tag{21}$$

[19] The fact that Λ is so small means that the melt pressure in the conduit is very close to magmastatic. Λ depends on the flux as $1/Q_0$, so a much lower flux would be needed in order to make it order 1. The fact that μ is small means that the temperature difference between the melt in the conduit and the walls is small. Thus as the wall temperature decreases up the conduit because of decompression, the melt temperature follows it, and the resulting energy flux into the walls is what causes them to melt. The situation is remarkably similar to that for channels of melt water in viscously deforming ice [*Nye*, 1976]. Neglecting these small terms of order μ and Λ causes θ to decouple and the channel equations (13)–(18) reduce to

$$\frac{\partial S}{\partial t} = M - S N_c, \tag{22}$$

$$\frac{1}{rSt} \frac{\partial S}{\partial t} + \frac{\partial Q}{\partial z} = \frac{1}{St} M + \Omega, \tag{23}$$

$$0 = 1 + \frac{\partial N_c}{\partial z}, \tag{24}$$

$$M - \frac{Q}{r} = 0 \tag{25}$$

These state that the channel opens and closes because of melting and viscous deformation, the melt flux increases because of melting of the walls and additional inflow through them, the melt pressure varies magmastatically, and the rate that the walls melt is given by the rate hot fluid is advected from below.

[20] Boundary conditions are required for the melt flux Q and the effective pressure N_c. For a channel extracting melt from partially molten rock we can expect the channel to grow by drawing in melt from the surroundings, so Ω is positive and we can prescribe $Q = 0$ at the bottom. If we envisage the channel extending through the full depth of the partial melt zone ($0 < z < 1$ in the nondimensional variables) this is at $z = 0$, and we can expect to prescribe a condition on the pressure at the top $z = 1$.

[21] It is not entirely clear what the appropriate condition here is, since what happens to melt at the top of the partially molten region is little understood. If a sufficient supply of melt comes up the conduit it could continue, perhaps

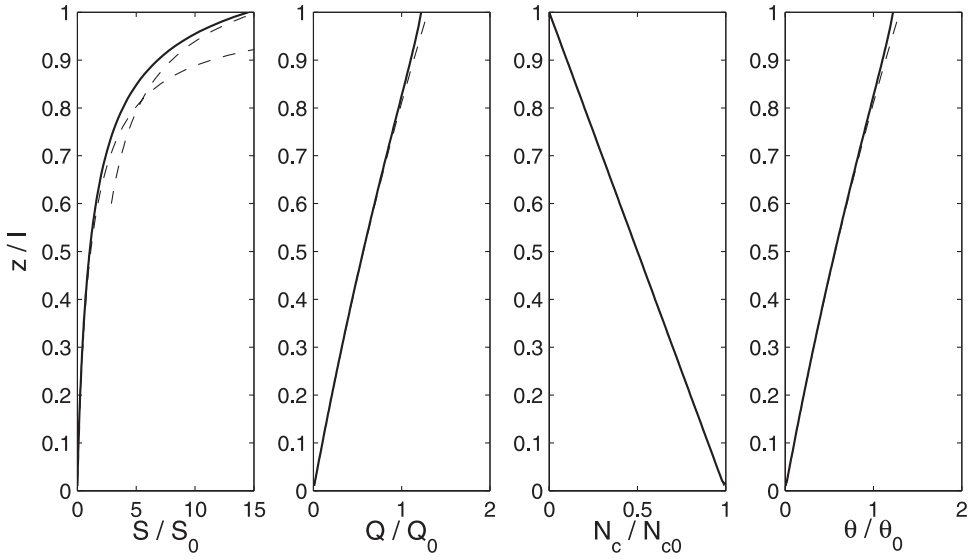

Figure 2. Steady state solutions to equations (13)–(18) and (26), for a constant influx $\Omega = 1$. The parameter values are $r = 1.2$, $St = 2$, $\Lambda = 5 \times 10^{-11}$, $\mu = 0.01$, $\nu = 0.7$. Dashed lines are the approximate solutions given by equations (27)–(30) and (36). The axes show the scaled variables, with the typical scales given in equation (20).

as a hydraulically driven fracture, up into the lithosphere to erupt on the ocean floor. Alternatively it might feed a sublithospheric magma chamber, or it might simply solidify. In the context of porous flow, *Hewitt and Fowler* [2008] suggested that the effective pressure should go to zero at the top of the partial melt, and we choose to satisfy the same condition here. If the conduit reached the open air, as is the case for subglacial melt channels reaching the snout of a glacier, this would certainly seem to be correct.

[22] Taking boundary conditions

$$Q = 0 \quad \text{at} \quad z = 0, \qquad N_c = 0 \quad \text{at} \quad z = 1, \tag{26}$$

gives the steady state solutions

$$Q = \int_0^z \Omega(\bar{z}) \exp\left(\frac{z-\bar{z}}{rSt}\right) \mathrm{d}\bar{z}, \tag{27}$$

$$M = \frac{Q}{r}, \tag{28}$$

$$N_c = 1 - z, \tag{29}$$

$$S = \frac{1}{r(1-z)} \int_0^z \Omega(\bar{z}) \exp\left(\frac{z-\bar{z}}{rSt}\right) \mathrm{d}\bar{z}, \tag{30}$$

which are shown in Figure 2. This suggests that the area of the channel grows without bound at the top $z = 1$ because there is no pressure difference to counteract melting with closure. This issue can be avoided if we allow the host matrix also to have some small vertical velocity, so that it, as well as the melt, is ascending. For a channel within the partially molten region beneath mid ocean ridges or in hotspots, this is indeed what is happening; the fact that the solid rock itself is ascending is the reason for decompression partial melting. The derivative in equation (13) is therefore really a material derivative, which we write (for consistency later) as

$$\frac{\partial S}{\partial t} + \varepsilon \delta_c^2 W \frac{\partial S}{\partial z} = M - S N_c, \tag{31}$$

where $\varepsilon \delta_c^2 W$ is the small vertical matrix velocity. Thus as S grows near $z = 1$, this extra advective term becomes important; the correction to the solution there can be found by rescaling

$$\begin{gathered} z = 1 - \varepsilon^{1/2} \delta_c W^{1/2} \hat{z}, \\ S = \frac{Q(1)}{r \varepsilon^{1/2} \delta_c W^{1/2}} \hat{S}, \quad N_c = \varepsilon^{1/2} \delta_c W^{1/2} \hat{N}_c, \\ Q = Q(1) \hat{Q}, \quad M = \frac{Q(1)}{r} \hat{M}. \end{gathered} \tag{32}$$

Then the leading order steady state equations (13)–(18) become

$$-\frac{\partial \hat{S}}{\partial \hat{z}} = \hat{M} - \hat{S} \hat{N}_c, \tag{33}$$

$$\hat{Q} = \hat{M} = 1, \tag{34}$$

$$\hat{N}_c = \hat{z}, \tag{35}$$

so $\hat{S}$ is given by

$$\hat{S} = \int_{\hat{z}}^{\infty} e^{(\hat{z}^2 - \hat{\zeta}^2)/2} \, \mathrm{d}\hat{\zeta} = \sqrt{\frac{\pi}{2}} e^{\hat{z}^2/2} \mathrm{erfc}\left(\hat{z}/\sqrt{2}\right). \tag{36}$$

This boundary layer solution is shown in Figure 2, and implies that the cross-sectional area at $z = 1$ tends to the finite dimensionless value $S = \sqrt{\pi/2}Q(1)/r\varepsilon^{1/2}\delta_c W^{1/2}$.

[23] If a channel can be supplied with a constant supply of melt from the surrounding porous melt, it can be expected to behave as in Figure 2; the flux is determined by the inflow as well as the additional production of melt caused by melting the walls; the pressure in the melt is nearly magmastatic; the temperature of the ascending melt closely follows the decreasing temperature of the walls by transferring its excess energy into melting; and the area of the channel adjusts so as to cause the rate of viscous closure to balance the melting rate in equation (13).

[24] It is worth pointing out that the nearly magmastatic conditions in the channel are a consequence of the dynamics, rather than an assumption. If the effective pressure were initially smaller, the melt would ascend much faster and consequently melt the walls faster, causing the channel to expand (equation (13)), and the effective pressure would evolve toward being magmastatic. The fact that the melt is so close to equilibrium means the channel area can be much larger than it would be under the full buoyancy force $\Delta\rho g$. Thus there is a typical radius of ~15 m (from (20)) even for a melt flux of only 0.01 m^3 s^{-1}.

[25] Finally, although the solution shown in Figure 2 is for a steady state channel extending the full depth of the partial melt, essentially the same behavior might be expected for a shorter channel. Non steady states are of course also possible, and in section 4 we see how a channel might "grow" downward into the partial melt.

3. Porous Flow Around a Channel

[26] The previous section describes the dynamics of a channel in a viscous medium undergoing decompression melting, but *assuming* that the channel is somehow fed by a supply of melt through its walls. We now attempt to explain this supply by examining the behaviour of the surrounding partial melt. The viscous matrix is really a porous compacting matrix, which is undergoing continual melting as it ascends. We have already seen that the melt pressure in the channel is nearly magmastatic, and thus significantly reduced from the lithostatic pressure in the matrix; thus if the far-field pore pressure in the melt is close to lithostatic, as we expect, the channel acts as a reduced pressure sink which can naturally be expected to draw in melt. The continual production of melt in the pores (caused by the background upwelling rate of the matrix) means the porous medium is not sucked dry but can provide a continued source of melt to the channel. To understand how this works we must first set out the principal dynamics governing the porous partial melt.

[27] Model equations have been set out numerous times in the past [*Ahern and Turcotte*, 1979; *McKenzie*, 1984; *Ribe*, 1985; *Fowler*, 1990a, 1990b; *Spiegelman*, 1993]. Until recently most analysis has tended to largely ignore the actual melting process and focus on the matrix compaction and how this affects the melt flow. Here, we take the simplest set of equations which we think capture the dominant physics, particularly the heat transfer from below which drives decompression melting. This means including the same physics as were included in the previous section for melt channels; mass conservation, energy conservation when the temperature is constrained thermodynamically to the pressure-dependent solidus, and a flow law, which in this context will be Darcy's law. These are expressed by

$$\frac{\partial\phi}{\partial t} + \nabla\cdot\phi\mathbf{u} = \frac{m}{\rho_l}, \tag{37}$$

$$-\frac{\partial\phi}{\partial t} + \nabla\cdot(1-\phi)\mathbf{V} = -\frac{m}{\rho_s}, \tag{38}$$

$$\begin{aligned} mL + (\rho_s c(1-\phi) + \rho_l c\phi)\frac{\partial T_s}{\partial t} \\ + (\rho_s c(1-\phi)\mathbf{V} + \rho_l c\phi\mathbf{u})\cdot\nabla T_s = 0, \end{aligned} \tag{39}$$

$$T_s = T_0 - \Gamma(p_l - p_0), \tag{40}$$

$$\phi(\mathbf{u}-\mathbf{V}) = \frac{k_0\phi^2}{\eta_l}(-\rho_l g\mathbf{k} - \nabla p_l), \tag{41}$$

Here ϕ is the volume fraction of melt, $\mathbf{V}$ and $\mathbf{u}$ are respectively the velocities of matrix and melt, and p_s and p_l are the pressures in matrix and melt. m (kg m^{-3} s^{-1}) is now the *local* melting rate and k_0 is a constant permeability coefficient. The heat capacity c is assumed to be equal in the two phases, and we ignore the effects of conduction and viscous dissipation in equation (38). Note that the temperature of melt and matrix is the same, and is determined by the interfacial pressure p_l according to the Clapeyron slope.

[28] The analogue of the closure relationship (4) for the porous region follows from applying the same law to individual pores, and results in a *compaction* relationship between the pressures

$$N \equiv p_s - p_l = -\frac{\eta_s}{\phi}\nabla\cdot\mathbf{V}, \tag{42}$$

where η_s/ϕ is the *bulk viscosity*, which describes how easily the combined matrix-melt structure can be deformed [*Batchelor*, 1967; *Sleep*, 1988].

[29] The missing equation is the total momentum conservation which we could write (ignoring inertia) as

$$0 = -\nabla p_s + \nabla(\phi N) - \rho_s g\mathbf{k} + \Delta\rho g\phi\mathbf{k} + \nabla\cdot(1-\phi)\boldsymbol{\tau}_s, \tag{43}$$

where $\boldsymbol{\tau}_s$ is the deviatoric stress in the matrix. However, we will assume here that this reduces to saying that solid pressure in the matrix is lithostatic,

$$p_s = p_0 - \rho_s g z. \tag{44}$$

Hewitt and Fowler [2008] nondimensionalized the equations and found that the viscous stresses caused only small perturbations to this in an ascending column of partial melt. The stresses which occur in a matrix undergoing corner flow beneath a spreading ridge are known to set up pressure

gradients which can drive some melt flow toward the ridge [*Spiegelman and McKenzie*, 1987; *Spiegelman*, 1993], but for the moment we ignore this effect and assume that the solid pressure is simply given by equation (44), as in section 2.

[30] The partial melt equations are scaled by assuming the upwelling rate W_0 is prescribed. With the length scale l, and writing the velocity scales as W_0 and w_0, a sensible choice is

$$T_{s0} = \Gamma \rho_s g l, \quad m_0 = \rho_s \frac{c\Gamma \rho_s g}{L} W_0, \quad t_0 = \frac{l}{W_0},$$
$$\phi_0 = \left(\frac{\eta_l}{k_0 \Delta\rho g} \frac{\rho_s}{\rho_l} \frac{c\Gamma \rho_s g l}{L} W_0 \right)^{1/2}, \quad N_0 = \frac{\eta_s}{l} w_0,$$
$$w_0 = \frac{k_0 \Delta\rho g}{\eta_l} \phi_0 = \left(\frac{k_0 \Delta\rho g}{\eta_l} \frac{\rho_s}{\rho_l} \frac{c\Gamma \rho_s g l}{L} W_0 \right)^{1/2}, \tag{45}$$

Note that the effective pressure N is scaled differently to the channel effective pressure N_c. As well as r and St given in equation (19) we define the new dimensionless parameters

$$\varepsilon = \frac{W_0}{w_0}, \quad \delta_c^2 = \frac{N_0}{N_{c0}}. \tag{46}$$

Notice that ϕ_0 could also be considered a dimensionless parameter, but it is related (by definition) to the others by $\phi_0 = \varepsilon r/St$. For simplicity we immediately make the Boussinesq approximation $r = 1$, and the equations can then be written as

$$\varepsilon \frac{\partial \phi}{\partial t} + \varepsilon \nabla.(\phi \mathbf{V}) + \nabla.[\phi(\mathbf{u} - \varepsilon \mathbf{V})] = m, \tag{47}$$

$$\nabla.[\phi(\mathbf{u} - \varepsilon \mathbf{V})] + St \nabla.\mathbf{V} = 0, \tag{48}$$

$$\phi(\mathbf{u} - \varepsilon \mathbf{V}) = \phi^2 \left(\mathbf{k} + \delta_c^2 \nabla N \right), \tag{49}$$

$$\nabla.[\phi(\mathbf{u} - \varepsilon \mathbf{V})] = \phi N, \tag{50}$$

$$m + \frac{\partial T_s}{\partial t} + \mathbf{V}.\nabla T_s + \frac{1}{St} \phi(\mathbf{u} - \varepsilon \mathbf{V}).\nabla T_s = 0, \tag{51}$$

$$T_s = -z. \tag{52}$$

[31] Taking $W_0 = 10^{-9}$ m s^{-1} $\approx$ 3 cm a^{-1} as a typical upwelling rate, and the other parameters in Table 1, gives

$$m_0 \approx 3 \times 10^{-11} \text{ kg m}^{-3} \text{ s}^{-1}, \quad \phi_0 \approx 0.005, \quad N_0 \approx 6.6 \times 10^6 \text{ Pa},$$
$$w_0 \approx 10^{-7} \text{ m s}^{-1} \approx 3 \text{ m a}^{-1}, \quad t_0 \approx 5 \times 10^{13} \text{ s} \approx 1.7 \text{ Ma}, \tag{53}$$

and

$$\varepsilon \approx 0.01, \quad \delta_c \approx 0.16. \tag{54}$$

ε is the ratio of solid velocity to melt velocity, so is always expected to be small. δ_c also being reasonably small is indicative of the fact that the pressure in the channel is reduced from that in the surrounding melt.

[32] The meaning of these equations is reasonably easy to see; the thermodynamic constraint (equation (52)) means that the energy equation (51) gives the melting rate m because of the upwelling rates of matrix and melt. This feeds into the mass conservation equation (47) to determine how the melt fraction evolves, with the divergence of melt being determined from Darcy's law (equation (49)). Equation (48) simply states that as the melt diverges the matrix must compact to replace it, and that compaction is governed through equation (50) by the effective pressure (hence also commonly called the *compaction* pressure). The fact that the effective pressure can then drive the melt flow in equation (49) allows for the possibility of melt flow focussing as we shall now see. It is immediately clear that the length scale over which this pressure has an effect is the compaction length

$$\delta_c l = \sqrt{\frac{k_0 \phi_0^2 \eta_s}{\eta_l \phi_0}} \approx 8 \text{ km}, \tag{55}$$

using the values in Table 1.

[33] Suitable boundary conditions are discussed by *Hewitt and Fowler* [2008]; we take a constant vertical upwelling rate W_0 to be prescribed at the bottom of the partial melt $z = 0$, where the melt fraction ϕ is zero. The effective pressure is prescribed to be zero at the top of the partially molten region, $z = 1$, where the melt reaches the lithosphere. The porous equations are simplified by writing the dimensionless matrix velocity as

$$\mathbf{V} = \mathbf{k} + \frac{1}{St} \nabla \mathcal{U}, \tag{56}$$

and combining the equations to get

$$\varepsilon \frac{\partial \phi}{\partial t} + \varepsilon \frac{\partial \phi}{\partial z} + \frac{\varepsilon}{St} \nabla \cdot (\phi \nabla \mathcal{U}) + \nabla.\left[\phi^2 \left(\mathbf{k} + \delta_c^2 \nabla N \right)\right] = 1 + \frac{1}{St} \frac{\partial \mathcal{U}}{\partial z} + \frac{1}{St} \phi^2 \left(1 + \delta_c^2 \frac{\partial N}{\partial z} \right), \tag{57}$$

$$\nabla.\left[\phi^2 \left(\mathbf{k} + \delta_c^2 \nabla N \right)\right] = \phi N = -\nabla^2 \mathcal{U}. \tag{58}$$

The boundary conditions are then

$$\frac{\partial \mathcal{U}}{\partial z} = 0, \quad \phi = 0 \quad \text{at} \quad z = 0,$$
$$\mathcal{U} = 0, \quad N = 0 \quad \text{at} \quad z = 1. \tag{59}$$

One-dimensional steady state solutions are shown in Figure 3. The melt rate is constant in this case, $m = 1$, and since ε is small in equation (47) it is largely balanced by melt divergence, which is buoyantly driven in equation (49). Thus apart from small boundary layers at the top and bottom, the melt fraction and melt velocity increase through the region as $z^{1/2}$.

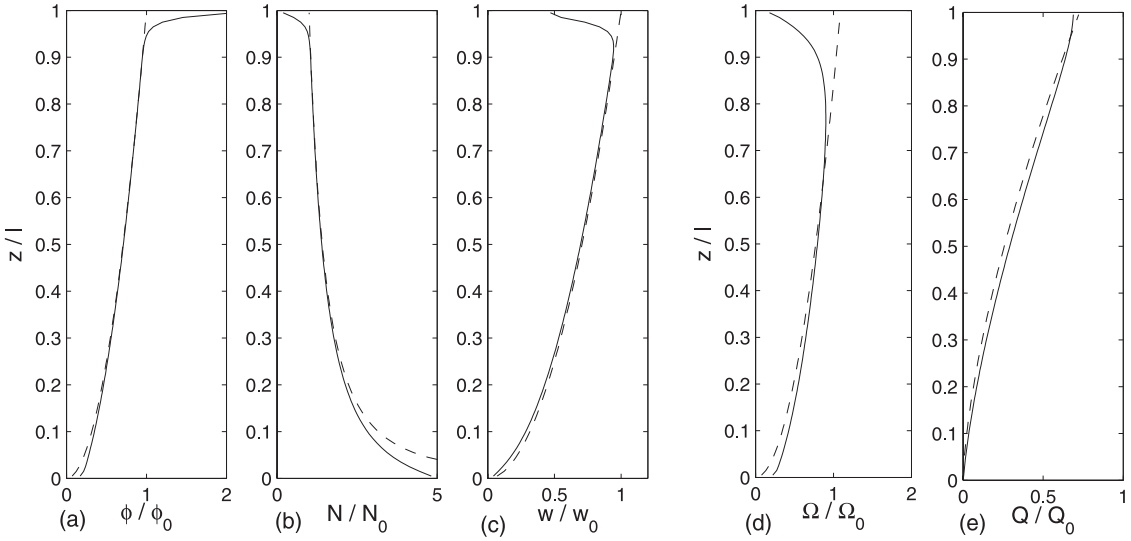

Figure 3. (a–c) One-dimensional solutions to equations (56)–(59) for an ascending column of partial melt. The parameters are $\varepsilon = 0.01$, $\delta_c = 0.14$, $St = 20$. Dashed lines show the approximate solutions $\phi = z^{1/2}$, $N = z^{-1/2}$, $w = z^{1/2}$. The axes show the scaled variables, with typical scales given in equation (53). (d–e) Influx and total flux for a channel of radius $r_c = 5 \times 10^{-4}$ as calculated by equation (62) from the numerical solution to equations (56)–(59) with equations (60) and (63) at the channel boundary. Parameters are $\varepsilon = 0.01$, $\delta_c = 0.14$, $St = 20$. Dashed lines show the approximate analytical solutions (73) and (74). The axes show the scaled variables with typical scales given in equation (61).

[34] We saw in section 2 that for a conduit of any appreciable size, the pressure in the channel is close to magmastatic. This means that the effective pressure in the matrix there, scaled as above with N_0, is $N = N_c/\delta_c^2$ with $N_c \approx 1 - z$ from section 2. This large effective pressure causes the melt flow in the surrounding porous region to be diverted toward the channel, and to calculate this flow we apply this channel effective pressure as a boundary condition; if a channel occupies the full depth of the partial melt, with dimensionless radius r_c, the boundary condition is

$$N = \frac{1-z}{\delta_c^2} \quad \text{at} \quad r = r_c, \tag{60}$$

where r is the radial coordinate, scaled with l and centered on the channel. A channel radius will be thin compared to the scale of the partial melt, so r_c is very small; as viewed by the partial melt, the channel is essentially a vertical line sink.

[35] We expect the channel to draw in melt from a surrounding region of radius comparable to the compaction length. The suitable scales for this influx and the total channel flux are therefore

$$\Omega_0 = \delta_c^2 l \phi_0 w_0 \approx 7 \times 10^{-7}\ \mathrm{m^2\ s^{-1}}, \quad Q_0 = \Omega_0 l \approx 0.035\ \mathrm{m^3\ s^{-1}}, \tag{61}$$

using the previously given estimates. With these scales, the radial influx to the channel will be

$$\Omega = -2\pi r_c \phi^2 \left.\frac{\partial N}{\partial r}\right|_{r_c}. \tag{62}$$

We know from earlier that the flow up the channel causes melting, which is balanced by the closure of the walls assuming the channel is in steady state. Using the scaling for Q_0 in equation (61), along with the results of section 2, this means that the boundary condition on the matrix velocity is

$$2\pi r_c \mathbf{V} \cdot \mathbf{n} = -\frac{\delta_c^2}{St^2} M \approx -\frac{\delta_c^2}{St^2}\frac{Q}{r}, \tag{63}$$

where M and Q are the scaled melt rate and volume flux in the channel, and $\mathbf{n}$ is the outward normal to the channel walls.

[36] Figure 4 shows a steady state numerical solution of equations (56)–(59) with equations (62) and (63) in which we take the channel radius r_c as fixed. The actual radius will need to depend on depth according to the channel dynamics, but for the purposes of seeing how the pressure sink affects the partial melt this is sufficient. The large effective pressure close to the channel causes enhanced matrix compaction there and results in a *decrease* in the melt fraction toward the channel; this decrease does not stop the melt from getting through however, as the pressure gradients driving it in are sufficiently high. The calculated influx Ω and resulting flux Q from such a solution are shown in Figure 3.

[37] Some straightforward analytical understanding of the flow into the channel can be seen if St is large, corresponding to the matrix undergoing only a small degree of melting. It is found numerically that the behaviour when St is smaller is not significantly different. Ignoring terms of order ε and $1/St$ in equations (56) and (58), the equations and boundary conditions are

$$1 = \nabla.\left[\phi^2\left(\mathbf{k} + \delta_c^2 \nabla N\right)\right] = \phi N, \tag{64}$$

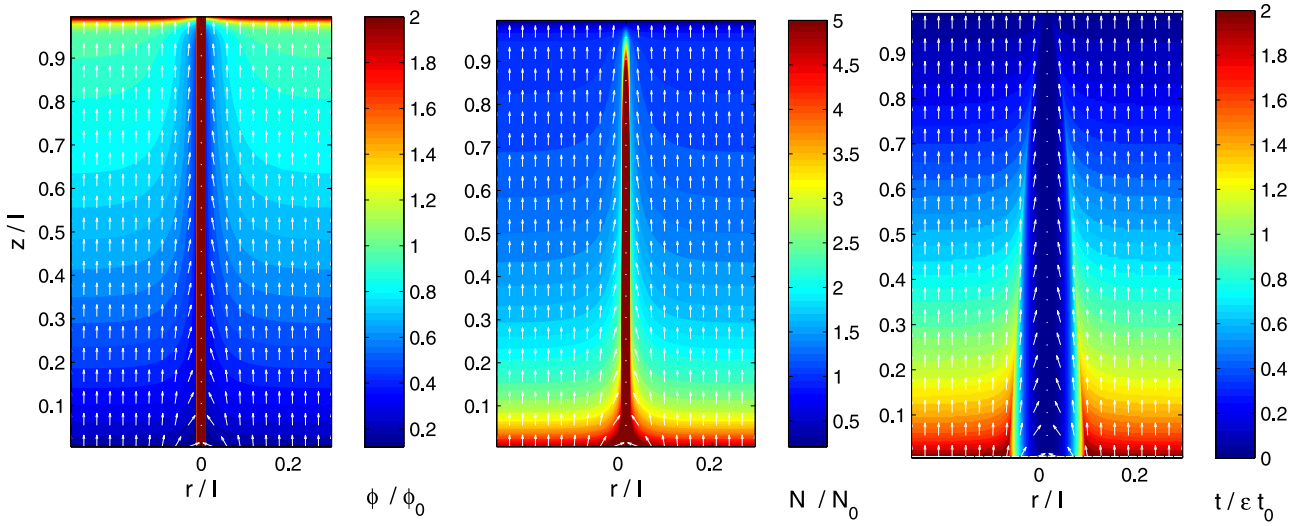

Figure 4. (a–b) Steady state solutions, for melt fraction ϕ and effective pressure N, to equations (56)–(59) with equations (60) and (63) at a channel boundary $r = r_c = 5 \times 10^{-4}$. White arrows show the direction of melt flow. The parameters are $\varepsilon = 0.01$, $\delta_c = 0.14$, $St = 2$. The variables are scaled with the typical values given in equation (53), and any values above the maximum on the color scale are colored the same. The melt fraction around the channel is very small (<0.5%). (c) Traveltime for melt to be extracted from the porous flow for the same situation. White arrows show the direction of melt flow. The time is scaled with the typical advective time in the partial melt $\varepsilon t_0 = l/w_0$.

$$N = \frac{1-z}{\delta_c^2} \quad \text{at} \quad r = r_c,$$
$$N \to \frac{1}{z^{1/2}}, \quad \phi \to z^{1/2} \quad \text{as} \quad r \to \infty, \tag{65}$$

which state that the melt divergence balances melting and is related to the effective pressure through the compaction law. The behaviour at infinity tends toward the one-dimensional solution. Thus $N = 1/\phi$, and ϕ satisfies a nonlinear reaction diffusion equation. Rescaling $r = \delta_c R$, and then taking only the leading order terms in δ_c, we have

$$2\phi\frac{\partial\phi}{\partial z} = 1 + \frac{\partial^2\phi}{\partial R^2} + \frac{1}{R}\frac{\partial\phi}{\partial R}, \tag{66}$$

$$\phi = 0, \quad \text{at} \quad R = R_c, \qquad \phi \to z^{1/2} \quad \text{as} \quad R \to \infty. \tag{67}$$

Approximate solutions to equations (66) are sought by writing $\phi = z^{1/2} + \psi$, and approximating

$$2\phi\frac{\partial\phi}{\partial z} \approx 2z^{1/2}\frac{\partial\phi}{\partial z} = \frac{\partial\phi}{\partial\xi}, \tag{68}$$

with the change of variable $\xi = z^{1/2}$. This is somewhat analogous to Oseen's approximation for flow past a sphere [*Batchelor*, 1967]. Then

$$\frac{\partial\psi}{\partial\xi} = \frac{\partial^2\psi}{\partial R^2} + \frac{1}{R}\frac{\partial\psi}{\partial R}, \tag{69}$$

$$\psi = 0 \quad \text{at} \quad \xi = 0,$$
$$\psi = -\xi \quad \text{at} \quad R = R_c, \qquad \psi \to 0 \quad \text{as} \quad R \to \infty. \tag{70}$$

Taking a Laplace transform gives the solution as

$$\psi = -\frac{1}{2\pi i}\int_{\gamma-i\infty}^{\gamma+i\infty} \frac{e^{p\xi}}{p^2}\frac{K_0\left(\sqrt{p}R\right)}{K_0\left(\sqrt{p}R_c\right)}\,\mathrm{d}p, \tag{71}$$

in terms of the modified Bessel function K_0. This can be used to calculate the flux into the channel from

$$\Omega = -2\pi r_c\phi^2\left.\frac{\partial N}{\partial r}\right|_{r_c} = 2\pi R_c\left.\frac{\partial\psi}{\partial R}\right|_{R_c}$$
$$= \frac{R_c}{i}\int_{\gamma-i\infty}^{\gamma+i\infty}\frac{e^{p\xi}}{p^{3/2}}\frac{K_1\left(\sqrt{p}R_c\right)}{K_0\left(\sqrt{p}R_c\right)}\,\mathrm{d}p. \tag{72}$$

If R_c is small, as we expect, asymptotic approximations to the Bessel functions can be used, and we find that the flux into the channel, scaled with Ω_0 in equation (61), is approximately

$$\Omega = 2\pi\frac{z^{1/2}}{-\ln\frac{R_c}{2} - \gamma}, \tag{73}$$

where $\gamma = 0.5772\ldots$ is the Euler-Mascheroni constant. This gives an integrated flux into the channel, scaled with Q_0 in equation (61),

$$Q = \frac{4\pi}{3}\frac{z^{3/2}}{-\ln\frac{R_c}{2} - \gamma}. \tag{74}$$

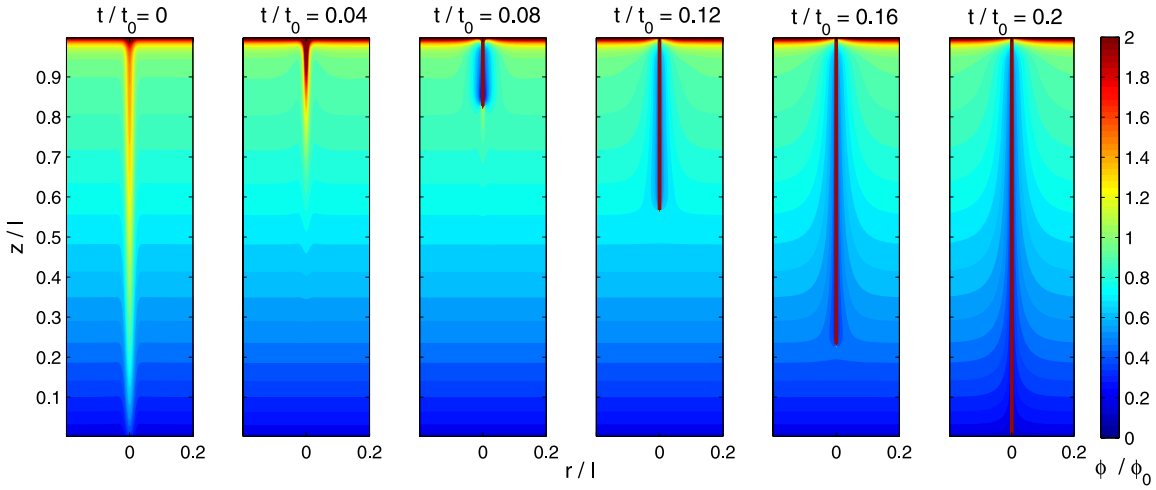

Figure 5. Evolution of melt fraction around a channel from a radially symmetric numerical calculation of equations (56)–(59), when the initial condition is the one-dimensional steady state with a Gaussian shaped perturbation added. The maximum initial porosity (scaled with ϕ_0) is around 2. Parameter values are $\varepsilon = 0.01$, $\delta_c = 0.14$, $St = 2$. All variables are scaled, with the typical scales in equation (53), and any scaled melt fraction larger than 2 is shown in red. When the melt fraction reaches 100% (corresponding to the scaled ϕ reaching 200), these cells are interpreted as channels as in section 2 and the pressure is prescribed to be magmastatic there. The boundary conditions (60) and (63) are then used.

Figure 3 shows these approximations in comparison with the numerical calculations. The effect of having *St* smaller is to cause a reduction in the melting rate close to the channel (because the melt is moving sideways and therefore not carrying so much heat down the solidus gradient), and thus a slight reduction in the influx from that given by equation (73). Nevertheless, equation (74) is quite a reasonable approximation for the total melt entering the channel.

[38] We see that a channel acts as a pressure sink to the porous flow, and can effectively suck out melt from a surrounding region on the order of the compaction length. This establishes the physical basis for the source term Ω to the channel in section 2; with the typical values used here, the flux in the channel (see Figure 3) is indeed of the order 0.01 $m^3\ s^{-1}$, as used there.

4. Channel Evolution

4.1. Radial Flow Into a Channel

[39] The models (13)–(18) for a melt channel and the models (47)–(52) for the partial melt are very similar and include the same physical mechanisms. The main difference between the two is that, whereas in the partial melt the melting rate is dominated by the upwelling of the *matrix*, in the channel it is dominated by the upwelling of the *melt*.

[40] In fact in the partial melt heat is carried upward by both the matrix *and* the melt; the flux carried by the melt is the $1/St$ term in equation (51). The Stefan number is thus the ratio of mass flux carried by matrix to melt; the smaller it is, the more the rock is ascending as melt rather than solid. Note that *St* is also a measure of the degree of melting, since $1/St$ is the fraction of rock which has melted by the time it reaches $z = 1$ in one-dimensional upwelling [see *Hewitt and Fowler*, 2008].

[41] The presence of the $1/St$ term in equation (51) allows for the possibility of a melting instability very similar to the reaction-infiltration instability [*Aharonov et al.*, 1995; *Kelemen et al.*, 1995; *Spiegelman et al.*, 2001]. That is; areas of larger melt fraction have a larger melt flux, which transports more heat upward and results in enhanced melting in those areas. This can have a runaway effect which causes the melt fraction to increase more and more, and eventually turn into an open channel. The dynamics of a high-porosity region within the partial melt, when the dominant advection term in equation (51) transfers from the matrix to the melt, vary smoothly toward those of the channel in section 2.

[42] Figure 5 shows the evolution of a small Gaussian perturbation to the one-dimensional steady state in the partial melt, from a numerical solution of equations (56)–(59). When the melt fraction reaches 100%, a channel is formed and the boundary conditions in equations (60) and (63) are used there. The initial perturbation increases the melt fraction by 50% of its undisturbed value to a maximum value of around 1%, and this perturbation is initially smoothed out by compaction over the majority of the region. However the low melt pressure in the higher porosity region near the top of the partial melt gradually pulls in more melt from the surroundings and as this melt becomes more and more localized it eventually channelizes. The channel then grows downward into the partial melt by drawing in melt from the sides and below, and eventually reaches the bottom, as was assumed in section 3.

[43] Since the average porosity in the partial melt is typically very small, the amount of melt available means the fully open channel must be extremely narrow compared to the scale of the partially molten zone, and also compared to the compaction length. Thus the resolution required to capture the growth of these channels in numerical simulations is quite high; the central cells in the discretization of Figure 5 have dimensionless radius 5×10^{-5}, and the channel is assumed to be contained within this.

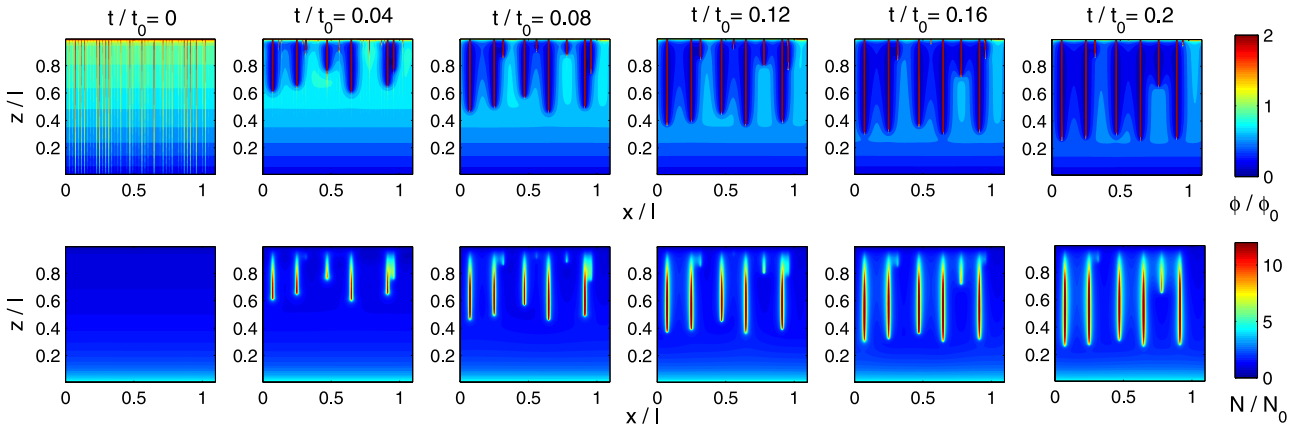

Figure 6. Evolution of ϕ and N in a two-dimensional numerical simulation of equations (56)–(59), with an initial condition consisting of the one-dimensional steady state perturbed by adding random amounts to the porosity in thin columns of cells with dimensionless width 10^{-4}. The maximum perturbed porosity (scaled with ϕ_0) is around 2. Boundary conditions in x are periodic, and the parameter values are $\varepsilon = 0.01$, $\delta_c = 0.14$, $St = 2$. All variables are scaled, with the typical scales in equation (53), and any scaled melt fraction larger than 2 is shown in red. If the melt fraction reaches 100% (corresponding to the scaled ϕ reaching 200), the equations no longer hold; such cells are interpreted as channels as in section 2 and the pressure is prescribed to be magmastatic there. Additional boundary conditions equivalent to equations (60) and (63) are therefore imposed. A characteristic spacing of channels similar to the compaction length develops, and the melt fraction between channels is very small (<0.5%). The channel growth downward is slowing toward the end, but this is a consequence of the resolution not being high enough to pick up the continued extension; the initial growth is nevertheless well resolved.

4.2. Two-Dimensional Flow Into a Channel

[44] The above section has all looked at radial flow into a cylindrical channel. We can analogously look at two-dimensional flow into a crack shaped channel, which extends a long way in the third dimension. If the breadth of the channel is b, one could expect the evolution equation equivalent to equation (4) for the crack width h to have the form [e.g., see *Sleep*, 1988]

$$\frac{\partial h}{\partial t} = \frac{M}{b\rho_s} - \frac{b}{\eta_s} N_c. \tag{75}$$

Such planar crack shapes might be expected if fracturing occurs in the mantle beneath mid-ocean ridges. Consideration of how the melting rate varies along the breadth of the crack suggests however that such a shape will be subject to instability, similar to the elastic fractures in the work of *Bruce and Huppert* [1989, 1990], and will naturally evolve toward a cylindrical shape instead.

[45] We would nevertheless like to show how the spacing of channels might evolve in a two-dimensional simulation (a larger three-dimensional simulation being beyond the scope of this paper), so we interpret the two-dimensional channels as behaving similar to those in section 2. There are some differences, particularly in the flow law which depends on h^3 rather than S^2, but essentially the dynamics are the same with S replaced by h. From the point of view of the partial melt, all that matters is that the channels act as line sinks of large effective pressure, since the melt pressure in the channel is again close to magmastatic; the precise shape of the channel does not alter this conclusion.

[46] Figure 6 shows a two-dimensional simulation of equations (56)–(59) (the background matrix motion is vertical so this might correspond to the plane along a midocean ridge axis rather than perpendicular to it), in which the one-dimensional steady state is perturbed by adding thin columns of larger porosity. The perturbations are randomly sized, but with a maximum disturbed porosity of around 1%. This initial condition is chosen because channels will only be resolved within very thin cells, so the perturbations are designed as seeds for potential channels within the thinnest cells in the discretization. Some of the perturbations disappear while others grow to form channels; as the incipient channels grow they try to draw in melt from their surroundings and consequently the larger ones grow at the expense of the smaller ones. A typical spacing of channels develops, of the order of the compaction length $\sim\delta_c l$, and the vast majority of the melt is focussed sideways into one of the channels.

5. Discussion

5.1. Melting Instability

[47] The dynamics of the channels presented here are somewhat different to the high-porosity channels which arise from mechanical instabilities [*Stevenson*, 1989; *Spiegelman*, 2003], decompaction beneath the lithosphere [*Sparks and Parmentier*, 1991] or reactive infiltration instabilities [*Kelemen et al.*, 1995; *Aharonov et al.*, 1995; *Spiegelman et al.*, 2001]; the destabilizing effect is very similar to that which causes reactive infiltration on a solubility gradient, but the local melting rate here continues to increase until an open channel forms. This is because increased melt flow enhances melting, and unlike in a

dissolution reaction, there is no limit to the amount of solid which can be "eroded".

[48] The instability seen in section 4 appears to be nonlinear, requiring a finite perturbation in melt fraction to initiate a channel; for larger Stefan numbers (corresponding to a lesser degree of melting) a larger perturbation is needed to initiate a channel. Substantial variations in melt fraction are presumably ubiquitous in the mantle (because of heterogeneities in composition for example), and if not, then the other instability mechanisms mentioned above may provide them.

5.2. Channel Flux and Spacing

[49] However they form in the first place, channels in a matrix undergoing decompression melting can be governed by the balance between viscous closure and melting. This allows for a steady state, and there seems to be no reason to suppose that these channels should not be long-lived features. The pressure in them is nearly magmastatic and therefore reduced from that in the surrounding pores, so they can continually suck in melt as fast as it is produced. The accumulation region is on the order of the compaction length, though as Figure 4 shows it is probably slightly smaller than this. Thus regardless of channel dynamics, the amount of melt which enters the channel can be expected to be comparable to that which is produced within a compaction length; this is exactly what the scaling in equation (61) says.

[50] The compaction length in the mantle is notoriously unknown, because of uncertainties and variability in properties such as the grain size and particularly the viscosities, which are also dependent on temperature, pressure, composition and volatile content. The values used above (Table 1) are rough estimates but in reality the viscosities of both magma and matrix may vary by at least an order of magnitude. Typical estimates for the compaction length range between 10 m and 10 km, with the most likely probably somewhere in the middle of this range. The flux in the channel is proportional to the square of the compaction length, so it similarly has a large range of uncertainty. In terms of the dimensional parameters it is, from equation (61),

$$Q_0 = \frac{r}{St}\delta_c^2 l^2 W_0 = \eta_s \left(\frac{k_0 \Delta\rho g}{\eta_l}\right)^{1/2} \left(\frac{\rho_s}{\rho_l}\frac{c\Gamma\rho_s g}{L}\right)^{3/2} l^{5/2} W_0^{3/2}. \tag{76}$$

5.3. Melt Velocities

[51] Some interesting features of the channels in section 2 to note are that the cross-sectional area, while very small in comparison to the scale of the melting region, is somewhat larger than one might imagine for the size of melt flux, with a diameter on the order of 30 m for a flux of order 0.01 m^3 s^{-1}. The melt velocity is seen from the definition of S_0 in equation (12), to be independent of the melt flux; the typical velocity is

$$w_{c0} = \frac{Q_0}{S_0} = \frac{\rho_s}{\rho_l}\frac{L}{c\Gamma\rho_s g}\frac{\Delta\rho g l}{\eta_s} \approx 300 \text{ m a}^{-1}, \tag{77}$$

using the values in Table 1. The flow is therefore much faster than the porous flow ($w_0 \approx 3$ m a^{-1}), but not enormous. In fact the channel really seems to act rather like a reservoir of melt, which is only slowly driven upward at the rate more melt is sucked in. (77) may be even faster than some geophysical constraints suggest [*Kelemen et al.*, 1997], but it is interesting to note from section 2 that the scaled velocity is roughly $Q/S = rN_c$ in the steady channel, and is therefore decreasing toward the top; thus (77) is probably an over estimate for the typical velocity.

5.4. Residence Times for Melt

[52] Examination of the timescales in sections 2 and 3 suggests travel times for melt to ascend the depth of the partial melt in a conduit may be only several hundred years, compared to 30 thousand years or more to rise the same distance by porous flow in the partial melt (these are estimates using the values in Table 1, so must be taken with due caution). Figure 4 shows the time taken for melt to be extracted from the partial melt, either into the channel or to the top of the region. It is seen that melt within the accumulation zone around the channel is relatively quickly drawn in, being in the partial melt for around 3 ka. Melt slightly further away appears to be retarded by the influence of the channel without being drawn into it, and takes longer to reach the surface than that furthest away which is unaffected by the presence of the channel.

5.5. Chemical Tracers

[53] Chemical feedbacks on the dynamics of the partial melt have been ignored in this study, but we can nevertheless consider the effect of this type of melt extraction on the concentration of tracer elements within the rocks. We consider simply idealized tracer elements which have a constant bulk partition coefficient κ, meaning that in equilibrium the concentrations in solid and melt must be in ratio $c_s/c_l = \kappa$. The porous flow is assumed to be entirely in chemical equilibrium, whilst an open channel will be assumed to be chemically isolated from the surrounding solid. The conservation equation

$$\frac{\partial}{\partial t}(c_l\phi + c_s(1-\phi)) + \nabla\cdot(c_l\phi\mathbf{u} + c_s(1-\phi)\mathbf{V}) = 0, \tag{78}$$

is solved for the concentrations in the case shown in Figure 4, and the results are summarized in Figure 7. The concentration in the channel is assumed to be well mixed; if on the other hand the chemical signal is preserved from when the melt entered the channel it might be expected that the more enriched melt from deeper in the mantle ascends in the center, with the melts from shallower nearer the edges [*Spiegelman and Kelemen*, 2003]; this would lead to more variability than is shown in Figure 7. It is however seen that the channel melt is enriched in incompatible elements with small bulk partition coefficients, whilst the melt in the surrounding residual matrix is relatively depleted.

5.6. Channel Alignment

[54] The channels studied here are all aligned vertically since the buoyancy force causes the melt to rise vertically. If variations in the matrix pressure caused by the viscous stresses in equation (43) were included, they would introduce an extra pressure gradient in Darcy's law (equation (49)), which effectively realigns the buoyancy force driving melt

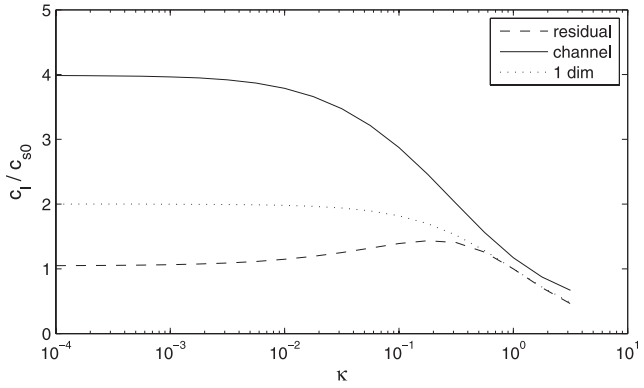

Figure 7. Concentration of an incompatible trace element in erupted melt compared to the concentration of the parent rock for different bulk partition coefficients $\kappa = c_s/c_l$. These are calculated using equation (78) from the radially symmetric steady state solutions to equations (56)–(59) with equations (60) and (63) at a channel boundary $r = r_c = 5 \times 10^{-4}$, as shown in Figure 4. The solid line shows the concentration in the melt at the top of the channel (which is assumed to be well mixed but not in chemical equilibrium with the surrounding rock), the dashed line shows the concentration in the melt in the residual matrix close to the top of the channel, and the dotted line shows the concentration in the melt at the top of a one-dimensional ascending porous column.

flow. In a matrix undergoing corner flow at a spreading ridge, these additional pressure gradients will be directed toward the ridge [*Spiegelman and McKenzie*, 1987], so channels which form might be expected to align themselves in the same direction. They could then provide an efficient mechanism to focus flow toward the ridge axis from a wider melting area.

5.7. Channel Interaction

[55] Intersection of two channels as investigated by *Ito and Martel* [2002] is a possibility, although they found that their dikes only interact over distances smaller than the compaction length, whereas the channels studied here have been seen to be spaced at this distance. As seen in Figure 6, closer channels do not want to coexist because the larger ones grow at the expense of the smaller ones by drawing in the surrounding melt.

6. Conclusion

[56] We have presented a mathematical model for melt flow in parts of the upper mantle and considered the possibility for open conduits of melt. This has been done in the context of a single component rock which melts because of decompression as it ascends. Unlike the usual models of these regions which concentrate on multiple components and dissolution reactions, we have included an energy equation which, because thermodynamic equilibrium is maintained, determines the rate of melting. This melting rate is not necessarily constant but is principally determined by the rate at which heat is carried upward by both matrix and melt; there may be some important consequences of this which are overlooked if a constant "background" adiabatic melting is assumed.

[57] The models presented here suggest that open melt channels might exist and be governed by (1) their growth caused by drawing in melt from a surrounding region of the order of the compaction length, and by melting the solid walls because of decompression melting; (2) their plastic closure, caused by pressure within the channel being almost magmastatic and therefore reduced from the lithostatic pressure in the surrounding matrix.

[58] Heat transfer occurs sufficiently fast that the melt in a channel would be roughly the same temperature as the surrounding matrix. A channel would be able to drain a surrounding region of the order of the compaction length, collecting a melt flux $Q \sim 0.01$ m^3 s^{-1} $\sim 3 \times 10^5$ m^3 a^{-1} for the values in Table 1, with ascent velocity on the order of 100 m a^{-1}. The surrounding residual matrix is reduced to very low melt fractions (<0.5%), and the melt from these regions is extracted into a channel in a few thousand years.

[59] Channels might naturally evolve from an instability very similar to the reactive infiltration instability associated with the heat transport by the melt, and will have a spacing comparable to the compaction length. They could act as a very efficient method for extracting melt and offer a physically grounded mechanism for near-fractional extraction.

[60] We do not claim that these types of channel necessarily exist in the mantle; but rather point out that the mechanisms to produce and maintain them are there. The models presented here are of course far too simplistic to capture everything that is going on beneath midocean ridges, and it is possible that other processes are dominant. However, it is interesting to observe that channels can form naturally during decompression melting even for a single component rock. Future work should look at modeling the melting of rocks with a more realistic composition, and determining the melting rate self-consistently.

Notation

b	Breadth of crack-shaped channel (m)
c	Specific heat capacity (J kg^{-1} K^{-1})
c_s	Tracer concentration in solid (mol m^{-3})
c_l	Tracer concentration in melt (mol m^{-3})
g	Gravitational acceleration (m s^{-2})
h	Width of crack-shaped channel (m)
$\mathbf{k}$	Unit vector in vertical direction (dimensionless)
k	Thermal conductivity (J m^{-1} s^{-1} K^{-1})
k_0	Permeability constant (dimensionless)
l	Depth scale of partial melt (m)
L	Latent heat (J kg^{-1})
m	Melt rate in partial melt (kg m^{-3} s^{-1})
m_0	Melt rate in partial melt scale (kg m^{-3} s^{-1})
M	Melt rate in channel (kg m^{-2} s^{-1})
M_0	Melt rate in channel scale (kg m^{-2} s^{-1})
N	Effective pressure in partial melt (Pa)
N_0	Effective pressure in partial melt scale (Pa)
N_c	Channel effective pressure (Pa)
N_{c0}	Channel effective pressure scale (Pa)
p_c	Melt pressure in channel (Pa)
p_l	Melt pressure in partial melt (Pa)
p_s	Matrix pressure (Pa)
p_0	Reference pressure (Pa)

Q Channel flux ($m^3\ s^{-1}$)
Q_0 Channel flux scale ($m^3\ s^{-1}$)
r Density ratio (dimensionless)
S Channel cross-sectional area (m^2)
S_0 Channel cross-sectional area scale (m^2)
St Latent heat/sensible heat (dimensionless)
T_s Solidus temperature (K)
T_{s0} Solidus temperature variation scale (K)
T_0 Reference temperature (K)
$\mathbf{u}$ Melt velocity in partial melt ($m\ s^{-1}$)
$\mathcal{U}$ Matrix velocity potential ($m^2\ s^{-1}$)
$\mathbf{V}$ Matrix velocity ($m\ s^{-1}$)
W_0 Upwelling velocity ($m\ s^{-1}$)
w_0 Melt velocity scale ($m\ s^{-1}$)
α Heat transfer constant (dimensionless)
Γ Clapeyron slope ($K\ Pa^{-1}$)
δ_c^2 Partial melt effective pressure/channel effective pressure (dimensionless)
ε Matrix velocity/melt velocity (dimensionless)
η_l Melt viscosity (Pa s)
η_s Solid viscosity (Pa s)
κ Bulk partition coefficient (dimensionless)
θ Excess temperature in channel (K)
θ_0 Excess temperature in channel scale (K)
Λ Viscous resistance/buoyancy in channel (dimensionless)
μ Excess temperature/solidus temperature range (dimensionless)
ν Viscous heating/advective heating in channel (dimensionless)
ρ_l Melt density ($kg\ m^{-3}$)
ρ_s Solid density ($kg\ m^{-3}$)
$\Delta\rho$ Density difference ($kg\ m^{-3}$)
$\boldsymbol{\tau}_s$ Matrix deviatoric stress (Pa)
ϕ Volume fraction of melt (dimensionless)
ϕ_0 Volume fraction scale (dimensionless)
ψ Porosity perturbation (dimensionless)
Ω Melt source to channel ($m^2\ s^{-1}$)
Ω_0 Melt source to channel scale ($m^2\ s^{-1}$)

[61] **Acknowledgments.** A.C.F. acknowledges the support of the Mathematics Applications Consortium for Science and Industry (www.macsi.ul.ie) funded by the Science Foundation Ireland mathematics initiative grant 06/MI/005. I.J.H. acknowledges the award of an EPSRC studentship. We thank the reviewers for their constructive comments on the manuscript.

References

Aharonov, E., J. A. Whitehead, P. B. Kelemen, and M. Spiegelman (1995), Channeling instability of upwelling melt in the mantle, *J. Geophys. Res.*, *100*, 20,433–20,450.

Ahern, J. L., and D. L. Turcotte (1979), Magma migration beneath an ocean ridge, *Earth Planet. Sci. Lett.*, *45*, 115–122.

Asimow, P. D., and E. M. Stolper (1999), Steady-state mantle-melt interactions in one dimension: I. Equilibrium transport and melt focusing, *J. Petrol.*, *40*, 475–494.

Batchelor, G. K. (1967), *Introduction to Fluid Mechanics*, Cambridge Univ. Press, Cambridge, U. K.

Bruce, P. M., and H. E. Huppert (1989), Thermal control of basaltic fissure eruptions, *Nature*, *342*, 665–667.

Bruce, P. M., and H. E. Huppert (1990), Solidification and melting along dykes by the laminar flow of basaltic magma, in *Magma Transport and Storage*, edited by M. P. Ryan, pp. 87–101, John Wiley, Chichester, U. K.

Fowler, A. C. (1990a), A compaction model for melt transport in the Earth's asthenosphere. Part I: The basic model, in *Magma Transport and Storage*, edited by M. P. Ryan, pp. 3–14, John Wiley, Chichester, U. K.

Fowler, A. C. (1990b), A compaction model for melt transport in the Earth's asthenosphere. Part II: Applications, in *Magma Transport and Storage*, edited by M. P. Ryan, pp. 15–32, John Wiley, Chichester, U. K.

Helfrich, K. R., and J. A. Whitehead (1990), Solitary waves on conduits of buoyant fluid in a more viscous fluid, *Geophys. Astrophys. Fluid Dyn.*, *51*, 35–52.

Hewitt, I. J., and A. C. Fowler (2008), Partial melting in an upwelling mantle column, *Proc. R. Soc. Ser. A*, *464*, 2467–2491, doi:10.1098/rspa.2008.0045.

Ito, G., and S. J. Martel (2002), Focusing of magma in the upper mantle through dike interaction, *J. Geophys. Res.*, *107*(B10), 2223, doi:10.1029/2001JB000251.

Iwamori, H. (1993), A model for disequilibrium mantle melting incorporating melt transport by porous and channel flows, *Nature*, *366*, 734–737.

Kelemen, P. B., J. A. Whitehead, E. Aharonov, and K. A. Jordahl (1995), Experiments on flow focusing in soluble porous media, with applications to melt extraction from the mantle, *J. Geophys. Res.*, *100*, 475–496.

Kelemen, P. B., G. Hirth, N. Shimizu, M. Spiegelman, and H. J. B. Dick (1997), A review of melt migration processes in the adiabatically upwelling mantle beneath oceanic spreading ridges, *Philos. Trans. R. Soc. London Ser. A*, *355*, 283–318.

McKenzie, D. (1984), The generation and compaction of partially molten rock, *J. Petrol.*, *25*, 713–765.

McKenzie, D. (1985), ^{230}Th-^{238}U disequilibrium and the melting processes beneath ridge axes, *Earth Planet. Sci. Lett.*, *72*, 149–157.

Nicolas, A. (1986), A melt extraction model based on structural studies in mantle peridotites, *J. Petrol.*, *27*, 999–1022.

Nye, J. F. (1953), The flow law of ice from measurements in glacier tunnels, laboratory experiments and the Jungfraufirn borehole experiment, *Proc. R. Soc. London Ser. A*, *219*, 477–489.

Nye, J. F. (1976), Water flow in glaciers: Jökulhlaups, tunnels and veins, *J. Glaciol.*, *17*, 181–207.

Olson, P., and U. Christensen (1986), Solitary waves propagation in a fluid conduit within a viscous matrix, *J. Geophys. Res.*, *91*, 6367–6374.

Ribe, N. M. (1985), The deformation and compaction of partial molten zones, *Geophys. J. R. Astron. Soc.*, *83*, 487–501.

Richardson, C. N., J. R. Lister, and D. McKenzie (1996), Melt conduits in a viscous porous matrix, *J. Geophys. Res.*, *101*, 20,423–20,432.

Röthlisberger, H. (1972), Water pressure in intra- and subglacial channels, *J. Glaciol.*, *11*, 177–203.

Sleep, N. (1988), Tapping of melt by veins and dikes, *J. Geophys. Res.*, *93*, 10,255–10,272.

Sparks, D. W., and E. M. Parmentier (1991), Melt extraction from the mantle beneath spreading centers, *Earth Planet. Sci. Lett.*, *105*, 368–377.

Spiegelman, M. (1993), Flow in deformable porous media. Part I: Simple analysis, *J. Fluid Mech.*, *247*, 17–38.

Spiegelman, M. (2003), Linear analysis of melt band formation by simple shear, *Geochem. Geophys. Geosyst.*, *4*(9), 8615, doi:10.1029/2002GC000499.

Spiegelman, M., and P. B. Kelemen (2003), Extreme chemical variability as a consequence of channelized melt transport, *Geochem. Geophys. Geosyst.*, *4*(7), 1055, doi:10.1029/2002GC000336.

Spiegelman, M., and D. McKenzie (1987), Simple 2-D models for melt extraction at mid-ocean ridges and island arcs, *Earth Planet. Sci. Lett.*, *83*, 137–152.

Spiegelman, M., P. B. Kelemen, and E. Aharonov (2001), Causes and consequences of flow organization during melt transport: The reaction infiltration instability in compactible media, *J. Geophys. Res.*, *106*, 2061–2078.

Stevenson, D. J. (1989), Spontaneous small-scale melt segregation in partial melts undergoing deformation, *Geophys. Res. Lett.*, *16*, 1067–1070.

Whitehead, J. A., and K. R. Helfrich (1986), The Korteweg-de Vries equation from laboratory conduit and magma migration equations, *Geophys. Res. Lett.*, *13*, 545–546.

A. C. Fowler, Department of Mathematics and Statistics, University of Limerick, Limerick, Ireland.

I. J. Hewitt, Mathematical Institute, University of Oxford, 24-29 St Giles', Oxford OX1 3LB, UK. (hewitt@maths.ox.ac.uk)